

AN EXPERIMENTAL STUDY ON LAMINAR-TURBULENT TRANSITION AT HIGH FREE-STREAM TURBULENCE IN BOUNDARY LAYERS WITH PRESSURE GRADIENTS

Bercelay NIEBLES ATENCIO¹, Valery CHERNORAY², Mohsen JAHANMIRI³

Abstract: *We report here the results of a study on measurements and prediction of laminar-turbulent transition at high free-stream turbulence in boundary layers of the airfoil-like geometries with presence of the external pressure gradient changeover. The experiments are performed for a number of flow cases with different flow Reynolds number, turbulence intensity and pressure gradient distributions. The results were then compared to numerical calculations for same geometries and flow conditions. The experiments and computations are performed for the flow parameters which are typical for turbomachinery applications and the major idea of the current study is the validation of the turbulence model which can be used for such engineering applications.*

1. INTRODUCTION

The laminar-turbulent transition has significant influence on determining the aerodynamic characteristics of immersed bodies such as evolution of losses, the appearance of separation and stall. Also, the transition behaviour has a dominant effect on the distributions of wall shear stress and surface heat transfer. To predict and manage the turbulence in different flow cases is beneficial for optimum advantage, namely, to reduce it when it is harmful (e.g. to decrease the skin friction or heat transfer) and to increase it when it is desirable (to avoid flow separation). The prediction of transition at high free-stream turbulence is of particular importance in turbomachinery where the boundary layer state defines the blade heat transfer and the flow separation margins.

In trying to understand the transition process, plenty of data and information has been collected from experiments on flat plates, but not much information and data has been collected and is available when it comes to understand the effect of free stream turbulence levels in the development of boundary layers along an airfoil or a vane, which is worthy to say that has a quite large application in engineering. Randomsky and Thole[1] presented measurements of the mean and turbulent flow field in the inviscid region of a turbine blade for low and highly turbulent flow field. They showed that in the inviscid region, the turbulent kinetic energy remains relatively high and also found some augmentation of the heat transfer near the leading edge and the pressure side as well, due to the high turbulence level.

¹ Chalmers University of Technology, Sweden, bercelay_niebles@yahoo.es

² Chalmers University of Technology, Sweden, Valery.chernoray@chalmers.se

³ Chalmers University of Technology, Sweden & Shiraz University of Tech., Iran, mohsenj1332@gmail.com

The nature of the transition itself allows the identification of turbulent/non-turbulent patterns which were first observed by Corrsin in 1943 [2]. This phenomenon was termed intermittency and later on, Kovaszny et al. [3] introduced the intermittency factor to identify turbulence, so that it is one when the fluid is turbulent and zero otherwise.

The effect of pressure gradients and turbulence levels on transition is best investigated by Abu-Ghannam and Shaw [4] proposing methods to calculate the momentum thickness Reynolds number for the start and the end of the transition zone, defined by them as the region in which the intermittency factor ranges between 0.25 and 0.75.

Walker and Gostelow [5] carried out experiments under high turbulence levels and adverse pressure gradients and found that close to the wall region within the boundary layer, a turbulent pattern was found to be not much affected by the free-stream conditions. The outer part of the boundary layer is more strongly affected by turbulence level and pressure gradient. Later, Gostelow et al. [6] found that at strong adverse pressure gradients, transition occurs quickly but it seems that the velocity profiles do not reflect this before the transition is completed. In another study, Salomon et al. [7] presented a new method for calculating intermittency in transitional boundary layers with rapidly changing pressure gradients, which is based on experimental studies using the pressure gradient parameter.

Mayle in his well-known paper, [8] mentions some experiments performed by Görtler in 1940 and Liepman in 1943, who analysed the effect of curvature on transition. From the experiments carried out by the latter, the transition Reynolds number depends on the turbulence level and on how strong the curvature is and seems to have a non-negligible effect in low pressure turbines and small engines, where a delay can be found. For compressors, the effects are negligible but still more data and studies are needed. In the same paper, Mayle keeps the discussion regarding the effect of curvature on transition and by using a curvature parameter, analyses its influence on transition Reynolds number.

Other researchers such as Bario and Beral [9] presented the results of their boundary layer measurements on pressure and suction sides of a turbine inlet blade and found on the pressure side that the onset of the transition, for low turbulence levels, occurs when Görtler vortices have been found. On the other hand, for high turbulence levels, the transition occurs at the beginning of the pressure side. The turbulence effect in the pressure side is considerable compared to that of the suction side. On the suction side, for low turbulence levels, the transition occurs before the flow may get separated and for higher levels of turbulence, the transition moves upstream to the leading edge.

Also, Van Treuren et al. [10] conducted experiments in the suction side of a low pressure inlet turbine for low free stream turbulence level and high free stream turbulence levels. In both cases they worked with low Reynolds numbers (25000 and 50000). At the lowest end of this range, they found strong and steady separation unable to be corrected either increasing the turbulence level or using vortex generator jets. When they worked with Reynolds number 50000, strong separation of the flow downstream the suction side of the vane was found for low free stream turbulence levels, but also they found opportunities to reattach the flow by introducing vortex generators and when increasing the turbulence levels.

In spite of the previously mentioned works, more information and study has to be performed in order to understand the effect of the different variables on the transition process over the airfoils, vanes and blades, which are, as previously said, present in many engineering applications. The aim of this project is therefore, to perform

experiments in the conventional wind tunnel of the Department of Applied Mechanics at Chalmers University of Technology with the help of the hot-wire measurement systems to investigate the effect of nose radius variation on the transition point and heat transfer rate of an ellipsoid to simulate and generalize the results.

2. EXPERIMENTAL SET UP

Experiments were performed in a linear cascade facility at Chalmers University. Figure 1 shows the configuration of this facility, which is of open circuit blower type and operates at velocities up to 20 m/s. The cross section of the working part of the facility is 200 by 1200 mm. The test-facility consists of a wide-angle diffuser, a settling chamber with a honeycomb and grids, a contraction, and a test section. A 30 kW fan is used to drive the flow.

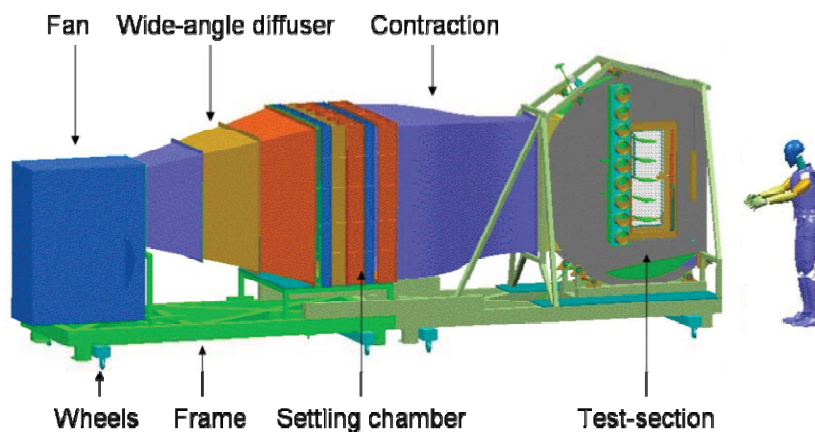


Figure 1: Test facility.

Figure 2 shows a sketch of the test section of the facility which is equipped with an end-wall boundary-layer suction system. Working flow incidence angles are designed to vary between 0 and 52 degrees relative to the axial inlet flow angle (for current experiments 0 degrees). A grid is used to create disturbances in the free stream and two turbulence intensities are procured for tests: 2% and 4%. For testing at 2% free stream turbulence intensity, the grid had to be placed at a distance "D" equal to 960 mm upstream from the point where $x=0$ (set up of coordinates explained later in this section). The grid then is moved so that $D=430$ mm, which is the distance needed to get 4% free-stream turbulence intensity. Different flow velocities (5, 9 and 18 m/s) are used and monitored using a Pitot-Prandtl tube connected to a digital micro-manometer, which also had sensors for temperature and absolute pressure readings.

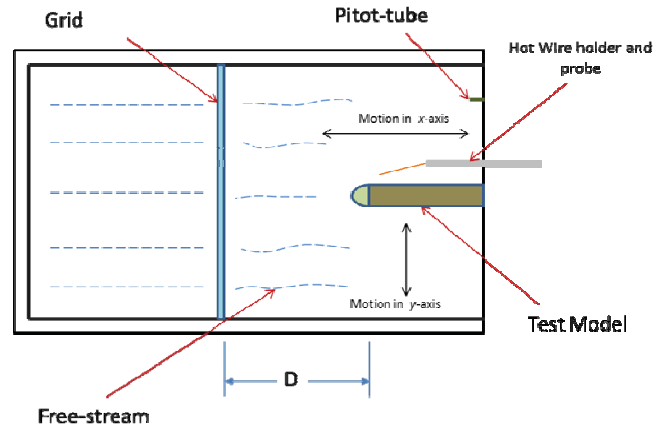


Figure 2: Sketch of the facility test section.

The probe positioning is controlled by an automated traversing system. In these experiments, the inputs received by this system were x , y , z coordinates and therefore the motion was 3-dimensional and performed by means of stepper motors with a resolution of $1.6 \mu\text{m}$. For each case, the x was in the streamwise direction. The y was perpendicular (vertical) to x . Preliminary tests were performed to assure two-dimensionality and it was found that velocity profiles along the z (spanwise direction) were quite uniform. For that reason, the experiments were carried out keeping a constant z -coordinate. As mentioned before, 3 different speeds were used and as described and shown later, 4 different noses were manufactured, which means 12 cases in total for the same free stream turbulence intensity. For each of the 2% free stream turbulence intensity cases, 16 different points along x -axis were taken for measuring and for each x -point, 27 points along the y -axis were determined, for a total of 432 x , y , z coordinates or measuring points. Figure 3 shows schematically the measurement points. For clarity, the vertical distances of shown measurement domain are stretched about three times. The noses are attached to a flat box. Therefore, their curved surfaces get flat progressively. At the point where the noses are coupled to the box, the surface is no longer curved and gets completely flat and the x - y coordinates are set to be zero ($x=y=0$). This means that the x -coordinates along the curved surface are negative and the x -coordinates along the flat box are positive. The $z=0$ (constant) is set by placing the probe in the middle of the spanwise length.

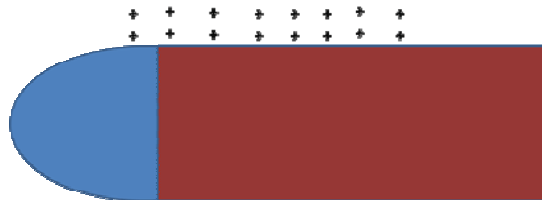


Figure 3: Illustrative sketch of typical measurement points over the complete test model.

The CTA anemometer was equipped with a tungsten wire of 3 mm length and $5 \mu\text{m}$ in diameter. The probe calibration was performed in a dedicated calibrator and the results of the calibration are stored in a file. The maximum error in the probe calibration was within 0.5% for all calibration points.

The experimental models were designed by using SolidWorks CAD software. The base configurations are two modifications of the NACA6 airfoil nose (a sharper modification and a more blunt modification). Two other models are created by changing the aspect ratio of the base configurations. The thickness-to-length ratio was decreased two times. Therefore, 4 different noses (for modelling of 4 different pressure gradients) were manufactured for testing. The resulting modified noses were named as 95N (large-scale sharp nose), 110N (large-scale blunt nose), 95sh (short version for 95N) and 110sh (short version for 110N). The flat part of the model is assembled by using plexi-glass plates and aluminium profiles. Figure 4 shows the differences in shapes for the noses, which result in different pressure gradients.

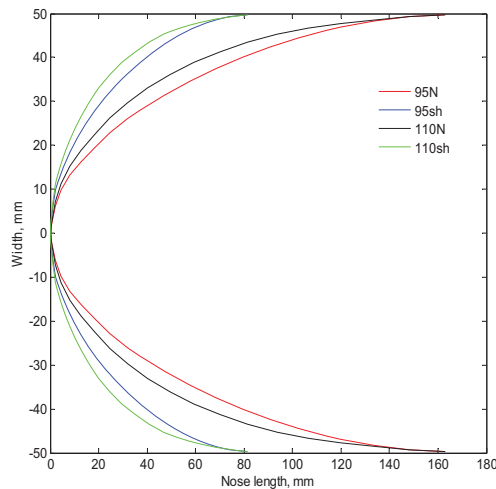


Figure 4: Shape of the noses used for the test models.

For every nose, 15 small holes (1.7 mm diameter) were designed in order to place pressure taps to monitor the static pressure distributions. Those taps are connected to a 16-channel PSI 9116 digital pressure scanner (Pressure System Inc.) which has a measuring range of ± 2500 Pa. The accuracy of the scanner in the measurement range of current experiment (± 250 Pa) is ± 2 Pa. Figure 5 illustrates the complete model.

As said earlier, probe positioning and data acquisition were fully automated and controlled by a PC with NI LabVIEW software. The software used for controlling motion is written using the LabVIEW graphical programming language, allowing the user to monitor current position, enter new coordinates and set speeds for each individual axis. Post processing of the experimental data was performed in Matlab (MathWorks Inc).



Figure 5: Real model showing the box and nose assembly.

The data was processed by using several written codes in Matlab (MathWorks Inc). At initial step the voltage data was converted to velocity with the help of a calibration file and major statistics is calculated, such as mean values and standard deviations. The resulting information was then stored for every case and contained values for Instantaneous velocities, Mean Velocities, The Root Mean Square of velocity fluctuations (rms) and Static Pressures. Further processing included computation of the boundary layer parameters, filtering and spectral analysis of data.

3. RESULTS AND DISCUSSION

Different pressure gradients acting on the model boundary layers are obtained by implementing different geometry of noses. Pressure distributions for each of the four models are shown in Figure 6. The pressure distributions for both large-scale noses (95N and 110N) and their short versions (95sh and 110sh) are shown in terms of the pressure coefficient, C_p versus $x-x_0$ (distance from leading edge).

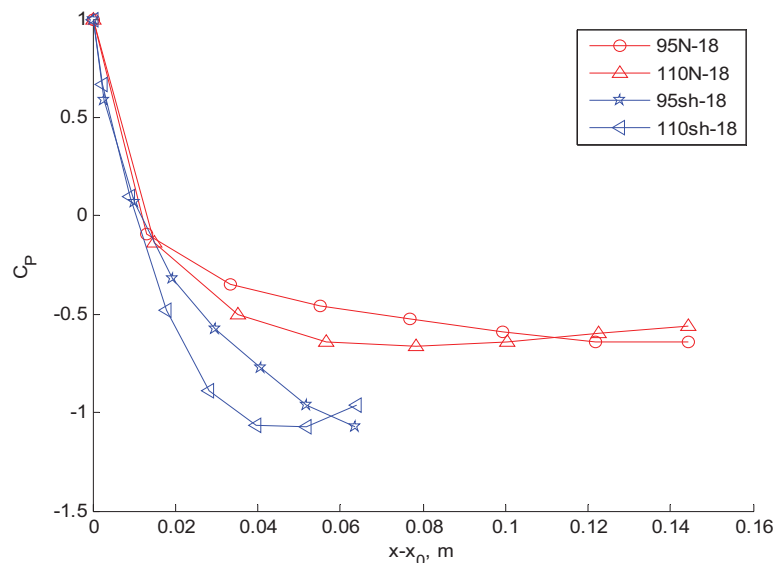


Figure 6: Static pressure distributions for the different models at 18m/s freestream velocity.

It is clearly seen that the 95-noses have the location of the pressure peak shifted downstream as compared to 110-noses and as a result the favourable pressure gradient extends up to the point of connection with the flat box.

For the 110-noses the adverse pressure gradient starts already on the nose itself. The 110sh nose causes the strongest favourable pressure gradient and for three other noses the favourable pressure gradient strength is decreased in the following order: 95sh, 110N, 95N.

Effect of flow Reynolds number (Re), pressure gradient and free stream turbulence intensity (Tu) on transitional flow were individually investigated as explained below.

3.1 Effect of Reynolds number

From the collected data, it is possible to plot velocity and rms profiles for all cases. In Figure 7, it is possible to see the velocity profiles obtained for the 95N, 5 m/s and 2% free stream turbulence intensity case (mild favourable pressure gradient and low flow Reynolds number) and profiles of rms of velocity fluctuations. From the mean velocity profiles plot it is possible to say that for the mentioned case, the flow starts behaving as laminar and not far from the Blasius profile. The Blasius solution can be seen depicted by a dashed line. Analysis of the profile shape factor, which will be given further, supports this fact as well. As we move downstream over the model, the flow changes gradually showing turbulent velocity profiles for the most downstream stations. The mean profiles for last two stations show noticeable similarity. The rms profiles at first stations show typical shape for laminar flow at high turbulence intensity. With increased downstream position the intensity of fluctuations increases until reaching a maximum at $x=90$ mm. From this position the maximum of rms is shifted towards the wall which is typical for turbulent boundary layer. From the rms profiles it is clearly seen that the turbulence intensity in the freestream is about 2%. Although the profiles give clues regarding the behaviour of the flow, boundary layer thickness and change from laminar to turbulent, they don't give clear quantitative information about where the transition is occurring.

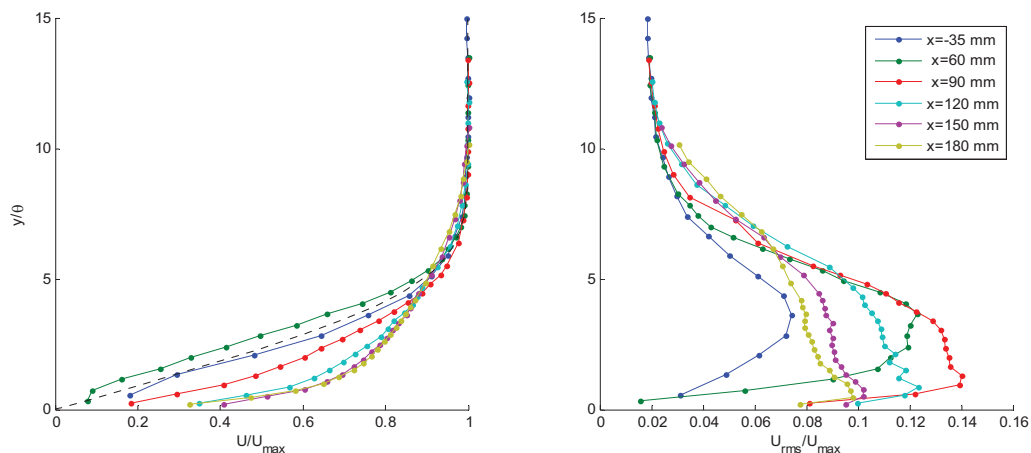


Figure 7: Velocity (left) and rms (right) profiles for nose 95N, 9m/s and freestream turbulence intensity, $Tu=2\%$

Contour plots of mean velocities and rms of velocity fluctuations were also obtained, to see more graphically the effects of different parameters on transition. Figure 8 shows a

contour plot of the mean velocity for the 95N case at different velocities. It is noticeable that the boundary layer is gradually becoming thinner and thinner as Re increases. Figure 9 shows, for the same case, how a turbulent region moves upstream as Re increases. It also shows that rms amplitude is higher when Re is higher.

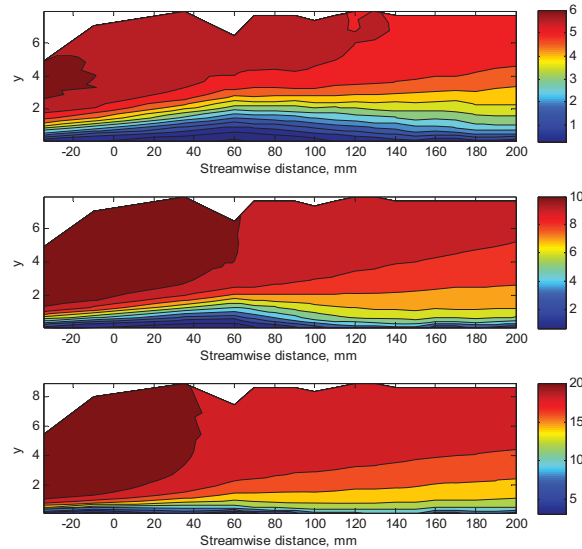


Figure 8: Mean velocities for the 95N nose. From top to bottom 5, 9 and 18 m/s.

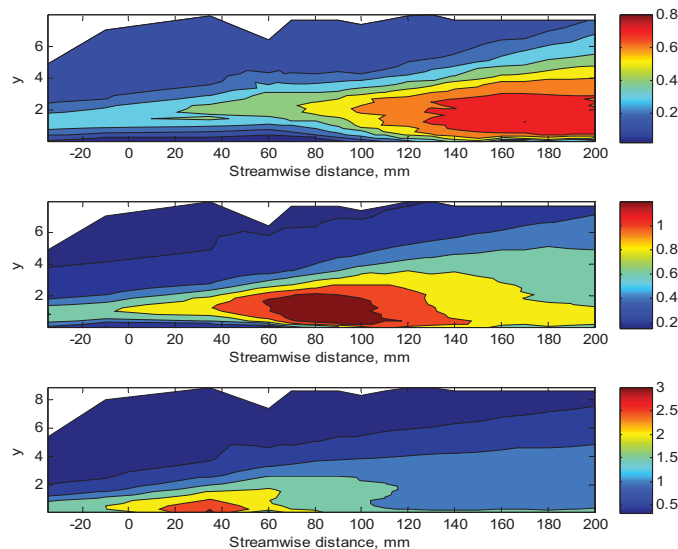


Figure 9: rms for the 95N nose. From top to bottom 5, 9 and 18 m/s.

According to Abu-Ghannam and Shaw [4], transition can be expressed in terms of Reynolds number based on the momentum thickness and the shape factor. For a certain flow condition, their paper shows that the transition onset is at the point where the shape factor starts decreasing. It is well-known [12] that for the Blasius boundary layer the shape factor is 2.59, for a boundary layer at the limit of separation the shape factor is 3.85 and for a turbulent boundary layer on a flat plate the shape factor is 1.3. Figure 10 shows two plots: the variation of the shape factor (H_{12}) and the rms of velocity fluctuations along the streamwise distance for the same cases mentioned previously (with nose 95N, different Re and $Tu=2\%$). Keeping in mind the experimental set up, the negative values for the streamwise distances in the plot correspond to the points along

the nose of the model (curved surface). From 0 (zero) on, the distances indicate those positions along the flat surface. From Figure 10 one can observe that H_{12} at $x=-20\text{mm}$ where the pressure gradient is zero is indeed very close to the value for Blasius boundary layer. At stations downstream, in adverse pressure gradient, H_{12} is increasing while is staying below the separation value of 3.85. At the most downstream positions, H_{12} is approaching value of 1.5 which is a typical value for a turbulent boundary layer. As can be seen from the plot, a drop in H_{12} for low and medium Re occurs more downstream than for the case at high Re (for 5 m/s this is occurring at around +70 mm, for 9 m/s occurring at around +40mm and at around -15 mm for 18 m/s). Moreover, the highest H_{12} is obtained for the lowest Re case, indicating that for this case, the risk of flow separation is the highest [11].

On the other hand, the *rms* plot of velocity fluctuations show peaks at different streamwise distances (for every case) which correspond to those points on the shape factor plot where the shape factor is reaching minimum values. The points at which these lower values of shape factor are obtained indicate those where it is possible to find turbulence and therefore, where the transition region ends. Finally, it is possible to note that the lowest Re produces the longest transitional region.

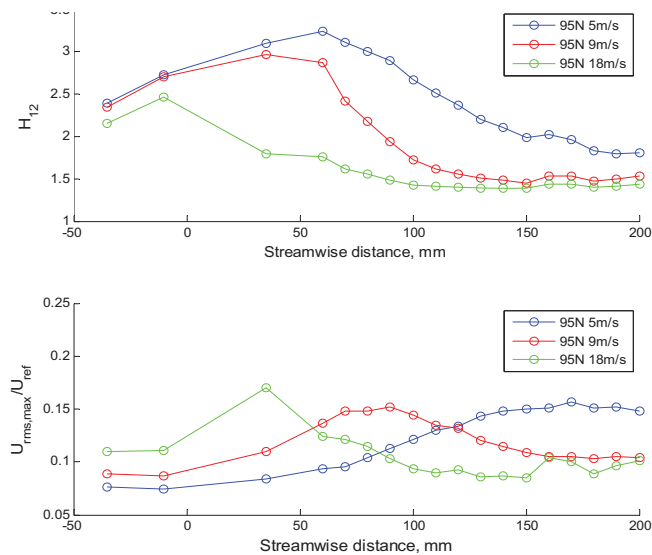


Figure 10: Shape factor (top) and *rms* plots (bottom) for the 95N nose. Different Re, and $Tu=2\%$

3.2 Effect of Pressure Gradient

The contour plots in Figure 11 show turbulence which is moving upstream when a stronger adverse pressure gradient is present. The level of maximum turbulence is also higher in that case, when compared to less strong adverse gradient case. Turbulence promotion is also observed in Figure 12, when the boundary layer is subjected to the strongest adverse pressure gradient. In Figure 13 the onset of transition is visualized in terms of shape factor (H_{12}) and *rms*. At the same speed and free-stream turbulence level, the effect of increasing the adverse pressure gradient is, as might be expected, an earlier transition beginning (when the shape factor starts decaying). The *rms* plot in same figure shows the peaks indicating the end of transition. By looking at the points where the transition starts and finishes, it is seen that the length of the transitional

region is also decreased in case of stronger adverse pressure gradient from 100 mm to 50 mm.

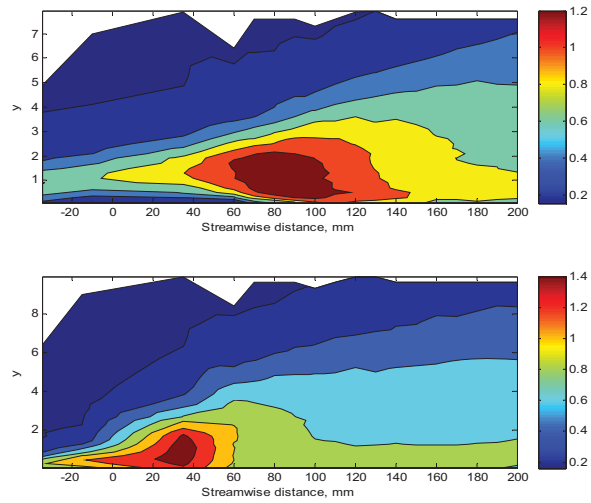


Figure 11: Turbulence promotion for different pressure gradient (95N top and 110sh bottom). Same Re (at 9 m/s) and Tu (2%).

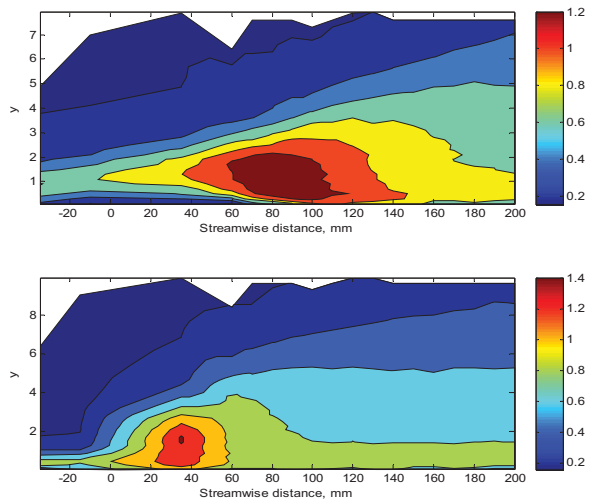


Figure 12: Turbulence promotion for different pressure gradients (95N top and 95sh bottom). Same Re (at 9 m/s) and Tu (2%).

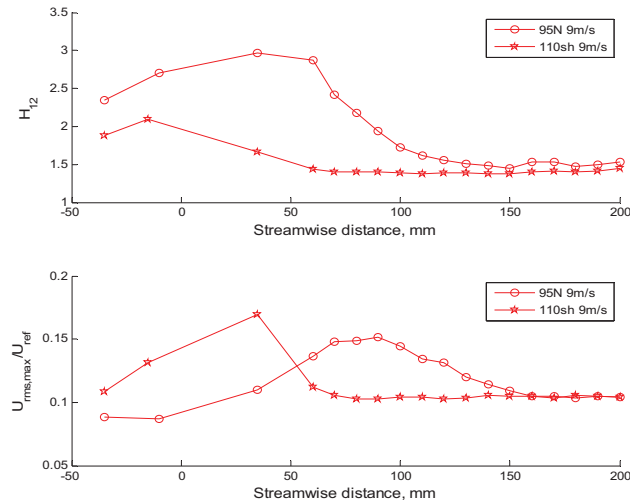


Figure 13: Shape factor and *rms* plots (top and bottom respectively) for same Re and Tu , but different pressure gradients.

In Figure 14, a comparison of the effects on the shape factor caused by different local Reynolds numbers and pressure gradients is shown. From this plot it is possible to observe that at stronger adverse pressure gradient the shape factor variation with changing of flow velocity is decreased.

The effect of pressure gradients on Reynolds number based on the momentum thickness Re_θ is shown in Figure 15. By observing the negative streamwise distances (from -50 to 0), it is easily inferred that Re_θ increases as the nose of the model is elongated. It is noticeable that for the short 110sh-nose, Re_θ has nearly the same values in the favourable gradient, at $x = -35$ for different velocities. As soon as the pressure gradient becomes adverse, the effect on Re_θ is greater and together with the flow velocity variation, the impact on Re_θ is much more noticeable.

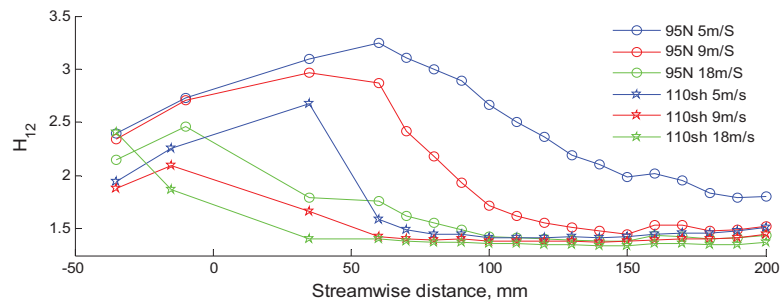


Figure 14: Comparison: Shape factors for different Re and pressure gradients.

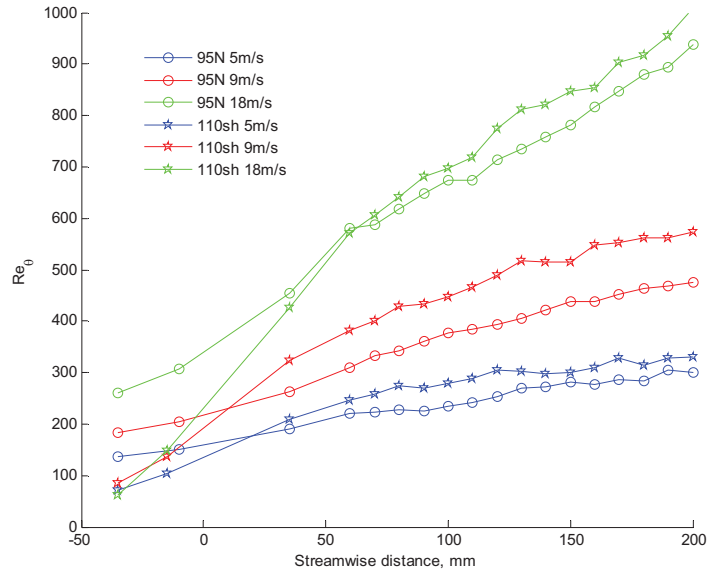


Figure 15: Reynolds number momentum thickness for same Tu , different speeds and pressure gradients.

3.3 Effect of Free-stream Turbulence Intensity

The plot in Figure 16 shows graphically how boundary layer turbulence varies when the free-stream turbulence is different. As it is expected, higher Tu promotes the transition onset. Figure 17 shows the shape factor (H_{12}) plot which confirms an earlier decay when increasing Tu . This plot also shows that for the same Re , H_{12} seems to be more sensitive to Tu effects, but for mild and higher Re , both the flow velocity and Tu have almost the same effect on H_{12} values and therefore, on transition inception.

In regards to the *rms* peaks, it is shown that the length of the transitional region seems to decrease as Tu is higher. It is noticeable that in the case of $Tu=4\%$ and highest velocity the transition occurs already in the zone of favourable pressure gradient.

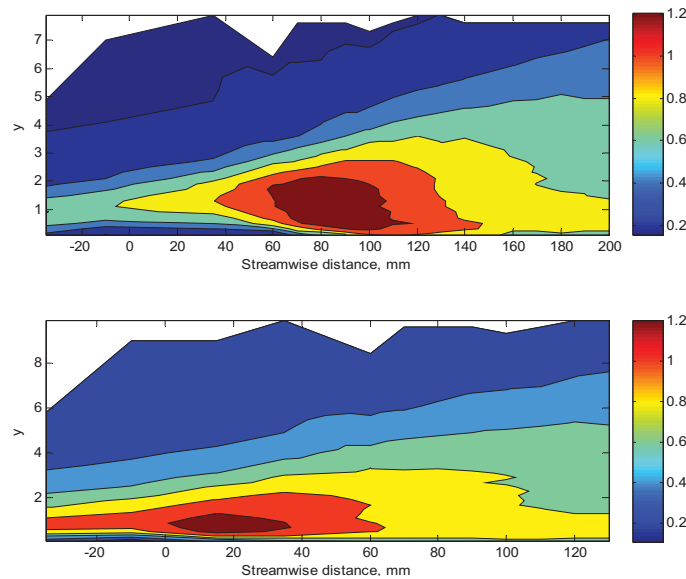


Figure 16: *rms* for different $Tu=2\%$ (top) and 4% (bottom). Same Re (at 9 m/s) and pressure gradient.

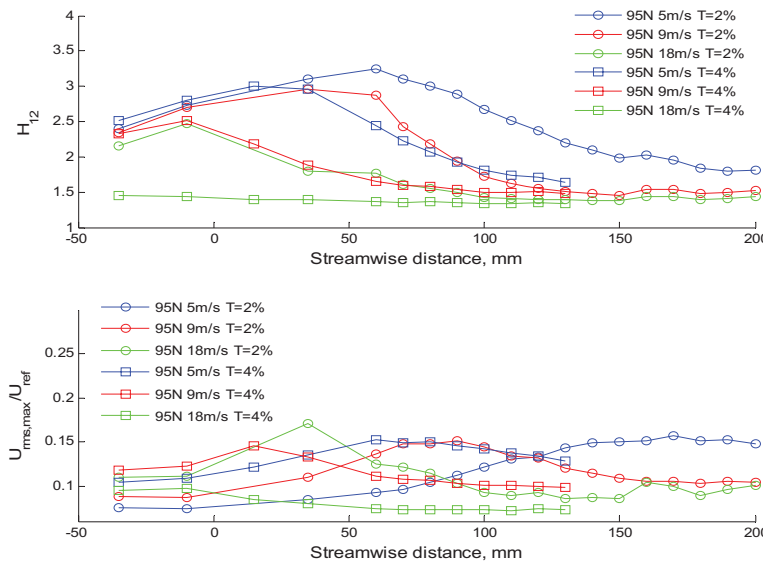


Figure 17: Shape factor and *rms* of velocity fluctuations (top and bottom respectively) influenced by free-stream turbulence intensity.

The next plot (Figure 18) shows that the pressure gradient effects have about same influence on the shape factor values as the effect caused by changing Tu for the same Re . It is noticeable that the peak value of the shape factor for a shorter nose is lower than the peak obtained for the longer nose with higher Tu . Moreover, the shape factor decay moves more upstream for the former case.

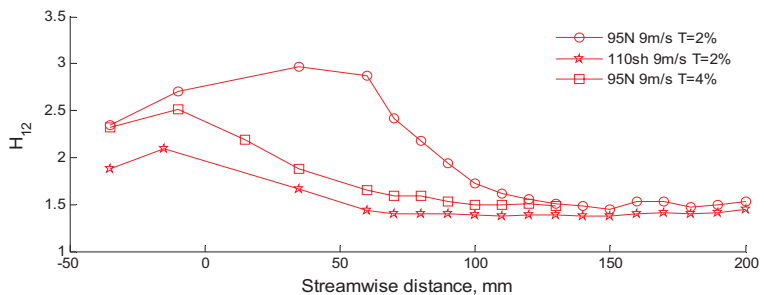


Figure 18: Comparison: effect of pressure gradient and Tu on shape factors at 9m/s.

Figure 19 shows the effect of free-stream turbulence intensity on Re_{θ} . At constant mild favourable pressure gradients, higher flow velocities together with higher free-stream turbulence intensity causes an increase in the Reynolds number momentum thickness. At low velocity, the free-stream turbulence intensity has about the same effect as the flow Reynolds number on Re_{θ} . As the streamwise distance is increased, the effect of the turbulence intensity of the free-stream on Re_{θ} becomes more pronounced.

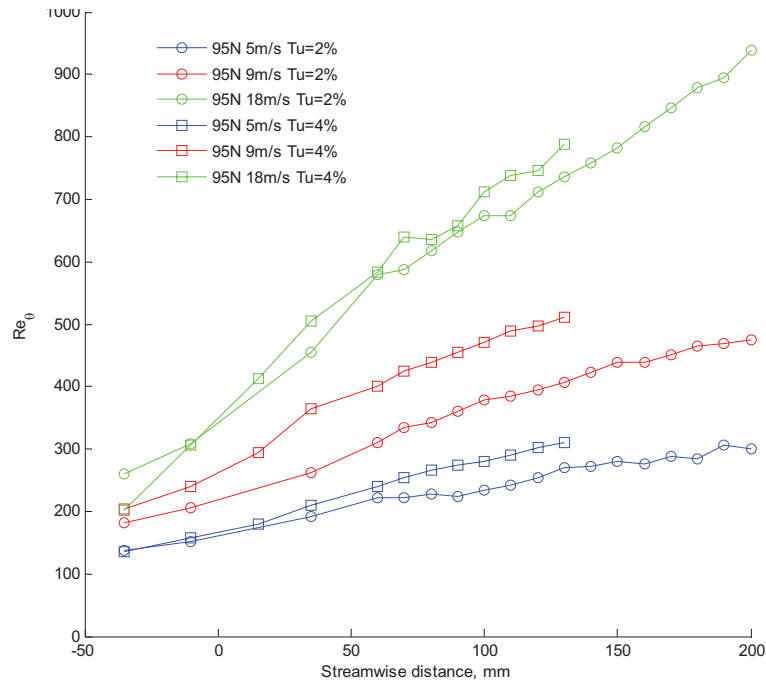


Figure 19: Reynolds number momentum thickness at different free-stream turbulence intensity and pressure gradients.

3.4 Comparison of CFD calculations and Experiments

It is well known that the simulation of laminar-turbulent transition is particularly challenging task for turbulence modelling. A number of turbulence models are developed which claim possibility of transition prediction and none of them is proven to be flawless so far. A relatively new transition model suggested by Langtry and Menter [13] was used in current study by means of ANSYS Fluent software. These numerical calculations were performed for same geometries as in experiments and were validated by using current experiments. The two-dimensional computations were performed. Structured computational meshes consist of 105 quadrilateral cells with an O-grid and resolved boundary layers surrounding the model. Pressure based implicit finite volume solver was used, and the discretisation schemes were second-order accurate. Calculations were performed with constant air properties. Boundary conditions in numerical calculations are matched with experimental conditions in the wind tunnel. At the inlet the velocity, turbulence intensity and the inlet turbulent length scale are set as in experiments.

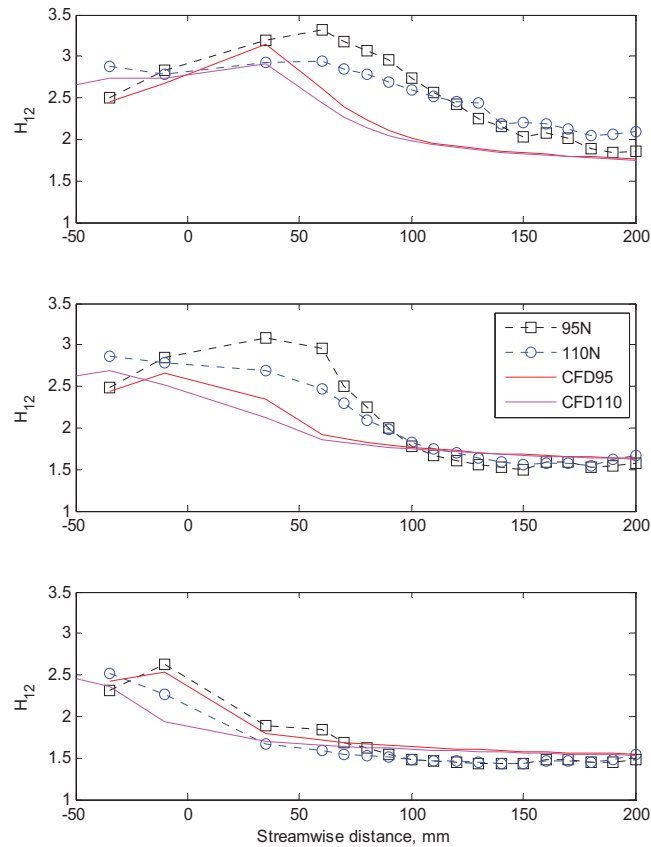


Figure 20: Comparison of CFD (lines) and experiments (symbols) for noses 95N and 110N at 5m/s, 9m/s and 18m/s (from top to bottom) and $Tu=2\%$.

Figures 20 to 22 show relevant results when CFD and experiments are compared. It is possible to see that for mild adverse pressure gradient, the predictions are quite good at high flow velocities (Figure 20). Rather good predictions are observed at all flow velocities and strong adverse pressure gradient (Figure 21). When the turbulence intensity is increased, the mid flow velocity and mild adverse pressure gradient case showed the best result (Figure 22). For $Tu=4\%$ and velocity of 9 m/s the transition occurs already in the zone of favourable pressure gradient. In this case the CFD is under predicting the transition. In general the CFD tends to over predict transition at mild adverse pressure gradients and to over-predict at strong adverse pressure gradient.

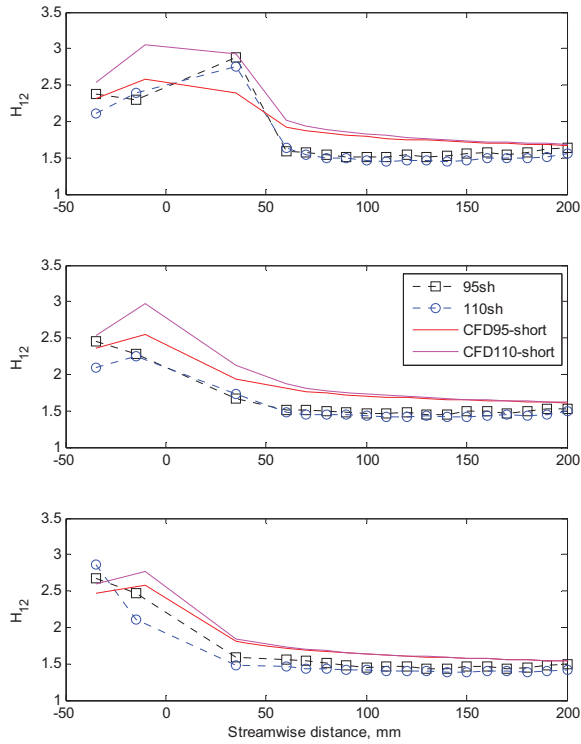


Figure 21: Comparison of CFD (lines) and experiments (symbols) for noses 95sh and 110sh at 5m/s, 9m/s and 18m/s (from top to bottom) and $Tu=2\%$.

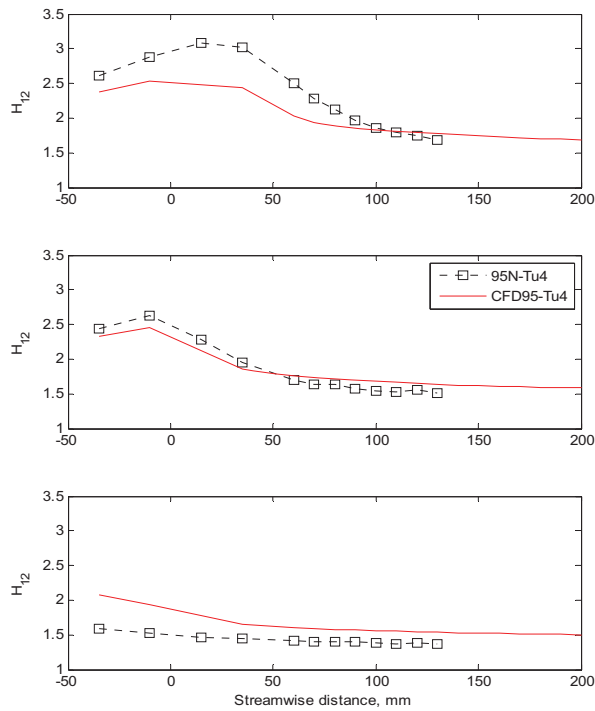


Figure 22: Comparison of CFD (lines) and experiments (symbols) for nose 95N at 5m/s, 9m/s and 18m/s (from top to bottom) and $Tu=4\%$.

4. CONCLUDING REMARKS

Laminar-turbulent transition at high free-stream turbulence in boundary layers of the airfoil-like geometries with presence of the external pressure gradient changeover has been studied experimentally. This study will help deepen our understanding of the transition phenomena especially for engineering applications.

The experimental data were collected for a number of flow cases with different flow Reynolds number, turbulence intensity and pressure gradient distributions. The flow parameters selected are typical for turbomachinery applications and many other engineering applications. A database for further studies and validation of numerical calculation is one of the major benefits.

The results from experiments show that the transition onset is promoted when the flow Reynolds numbers and the free-stream turbulence intensity are increased. This happened even when the boundary layers are subjected to strong favourable pressure gradients and adverse pressure gradients.

Preliminary numerical calculations for same geometries and flow conditions as in experiments by using SST model with transition by Langtry and Menter were tested. CFD shows rather good prediction of transition location for cases with strong adverse pressure gradient for both studied turbulence levels. In cases of mild adverse pressure gradient CFD computations demonstrate a satisfactory prediction with some under- or over-prediction of the transition onset.

In order to validate further performance of numerical tools for transition modelling, more studies involving the measurements and computations of heat transfer are suggested for future work.

REFERENCES

- [1] Radomsky R.W., Thole K.A.: "Flowfield Measurements for a Highly Turbulent Flow in a Stator Vane Passage", ASME Journal of Turbomachinery 122, p. 255-262, April 2000.
- [2] Corrsin S.: "Investigation of flow in an axially symmetrical heated jet or air". NACA, Wartime Report, W-94, 1943.
- [3] Kovaszny L.S.G., Kibens V. and Blackwelder R.F., "Large-scale motion in the turbulent boundary layer" J. Fluid Mechanics 41, p.283, 1970.
- [4] Abu-Ghannam B.J., Shaw R.: "Natural Transition of Boundary Layers-The Effects of Turbulence, Pressure Gradient, and Flow History", IMechE Journal Mechanical Engineering Science 22, p. 213-228, 1980.
- [5] Walker G.J., Gostelow J.P.: "Effects of Adverse Pressure Gradients on the Nature and Length of Boundary-Layer Transition", ASME Journal of Turbomachinery, 112, p. 196-205, 1990.
- [6] Gostelow J.P., Blunden A.R. and Walker G.J.: "Effects of Freestream Turbulence and Adverse Pressure Gradients on Boundary-Layer Transition", ASME Journal of Turbomachinery, 116, p. 392-404, 1994.

- [7] Solomon W.J., Walker G.J. and Gostelow J.P.: "Transition Length Prediction for Flows with Rapidly Changing Pressure Gradients", ASME Journal of Turbomachinery, 118, p. 744-751, 1996.
- [8] Mayle R.E.: "The 1991 IGTI Scholar Lecture: The Role of Laminar-Turbulent Transition in Gas Turbine Engines", ASME Journal of Turbomachinery 113, p. 509-537, October 1991.
- [9] Bario F., Beral C. : "Boundary layer measurements on the pressure and suction sides of a turbine inlet guide vane", Experimental Thermal and Fluid Science 17, p. 1-9, 1998.
- [10] Van Treuren K. W., Simon T., Von Koller M., Byerley A. R., Baughn J. W., Rivir, R.: "Measurements in a turbine cascade flow under ultra-low Reynolds number conditions" ASME Journal of Turbomachinery , 124 p. 100-106, January 2002.
- [11] Web site: http://www.cortana.com/Drag_Description.htm
- [12] Schlichting H., Boundary Layer Theory, McGraw-Hill, 1979.
- [13] Langtry R.B. and Menter F. R.: "Transition Modelling for General CFD applications in Aeronautics", AIAA 2005-522, 2005.